

# Correlation Between Heat Input and Mechanical Properties of Submerged Friction Stir Processed TIG-Welded AA8011/AA6082 Dissimilar Joint: Sampling Aspect

Velaphi Msomi<sup>1\*</sup>, Sipokazi Mabuwa<sup>1</sup>, Ali Merdji<sup>2</sup>

1. Cape Peninsula University of Technology, Mechanical and Mechatronic Engineering Department, Faculty of Engineering and the Built Environment, Bellville Campus, South Africa
2. Department of Mechanical Engineering, Faculty of Science and Technology, University Mustapha Stambouli of Mascara, Algeria

\* Corresponding Author: Email:msomiv@gmail.com

## Abstract

*This paper reports on the relationship between heat input and microstructure of the submerged friction stir processed TIG-welded AA8011/AA6082 dissimilar joint. The AA8011/AA6082 dissimilar joint was produced through the tungsten inert gas (TIG) technique before processing. The dissimilar welded joint was then subjected to a friction stir processing (FSP) technique that was fully submerged underwater. The temperature profile was measured using the K-type probes installed along the joint, and the properties of the joint were studied using various laboratory equipment. The variation in heat input was studied in correlation with the microstructural arrangement. The thermal instability was observed at the start of the joint, while thermal stability was observed from the middle to the end of the joint. The average grain size ranged between 5  $\mu\text{m}$  and 8  $\mu\text{m}$ : the average grain size of 8  $\mu\text{m}$  was measured on the sampled specimen from the start of the joint, while 5  $\mu\text{m}$  was measured on the sampled specimen from the end of the joint. The tensile properties of the joint increased gradually along the joint. The ultimate tensile strength (UTS) recorded for the sampled specimen from the start of the joint was 76.9 MPa with a percentage elongation of 8.79%, while that of the sampled specimen from the middle of the joint was 80.3 MPa with a percentage elongation of 21.82%, and the UTS for the sampled specimen from the end of the joint was 87.2 MPa with a percentage elongation of 24.12%. The microhardness at the stir zone of the joint varied between 52 HV and 64 HV; these values were lower than AA6082 base metal but higher than AA8011 base metal. The lower microhardness value corresponds to the sampled specimen from the start of the joint, while the higher microhardness value corresponds to the sampled specimen from the end of the joint.*

**Key Words:** Thermal history, microstructure, friction stir processing, 8011 aluminum alloy, 6082 aluminum alloy

## 1. Introduction

Friction stir processing (FSP) modifies the microstructure of materials through a rotating tool [1]. It works with a principle comparable to that of friction stir welding (FSW); however, FSP does not join materials because it works with a single surface [2]. FSP technique is categorized as the new microstructural modifying method that has shown significant plausible application [3]. The fact that FSP modifies microstructure suggests that it can enhance several metals' properties [4,5]. Additionally, recent studies have validated that FSP is capable of producing surface composites via the incorporation of particles [6,7]. Recent works have revealed that FSP parameters depend on the material being processed, i.e., the parameters used in processing certain grades of aluminum will be different from parameters used in processing

magnesium grades [8,9]. The variation of FSP parameters has resulted in a range of research meant to optimize this technique. This includes analyzing the impact of rotational, traverse speed, tool profile, and ambient conditions on properties of the friction stir processed material [10,11]. The following are several recent studies conducted on the subject of FSP technology which are investigating various aspects of this technology.

Yang et al. [12] have employed the multi-pass submerged FSP technique to produce composites from AA5083 and AlCoCrFeNi high entropy alloy particles (HEA). The pin-less tool was used to enclose HEA particles deposited on the surface of AA5083 before conducting processing. The enclosure of HEA particles was followed by the employment of a five-pass submerged FSP

procedure. Microstructural analysis revealed a uniform distribution of HEA particles in the composite produced through the five-pass FSP procedure. Good metallurgical bonding between the HEA particles and the matrix with refined grains was also observed from the same composite. The wear resistance and the microhardness of composites improved significantly compared to the as-received AA5083. The same multi-pass FSP technique was also employed by Xue et al. [13] on the copper plate (Cu). However, Xue et al. did not use the technique to produce composite but to study the mechanical properties of the zones between the overlapping FSP passes of Cu (called transitional zones [TZ]). There was no significant grain size difference between the transitional zones and the stir zones of the overlapping FSP passes. The microhardness of the friction stir processed area was uniformly low due to softening dominating the transitional zones.

Feng et al. [14] have conducted submerged FSP on AA2219-T6 using constant traverse speed and varying rotational speed. The grain size of the processed zone was smaller than that of the base metal, but the microhardness of the processed zone was lower than that of the base metal. This behavior was attributed to the formation (instead of dissolution) of the incoherent equilibrium  $\theta$  precipitates from base metal  $\theta'$  precipitates. Chai et al. [15] have investigated the microstructure and tensile properties of AZ91 magnesium friction stir processed underwater and under a normal air environment. The microstructural analysis revealed refined grains of the stir zone produced from submerged FSP compared to those of the stir zone produced from normal FSP. The tensile strength and elongation of the AZ91 alloy processed underwater were higher than the AZ91 alloy processed under normal air. It was also observed that the tensile strength of AZ91 alloy processed underwater was three times more than the base metal. The grain refinement of austenitic stainless steel was achieved by Selvam et al. [16] when the FSP was performed underwater rather than in normal air conditions. The hardness of the processed steel was higher than the base metal, but a decrease in elastic modulus was observed on the processed steel. This behavior was attributed to the texture evolution occurring during processing. The wear and erosion resistance were found to be improved post-processing, with more improvement observed from specimens processed in underwater conditions.

Darras and Kishta [17] have performed FSP on AZ31 magnesium alloy using three different media i.e., air, hot water, and cold water.

Significant grain refinement was observed on specimens produced under cold water conditions. The thermal profiles for the three conditions were also studied comparatively. The peak temperature of the cold water FSP was the lowest compared to the other FSP conditions. The cooling rate for cold water FSP was also higher than of the other FSP conditions. The tensile strength and yield strength of the specimens processed under three conditions were lower than the base metal. However, the elongation of each of the three specimens was higher than the base metal, with specimens processed under hot water the highest.

Cao et al. [18] have utilized submerged FSP to produce ultra-fine grained Mg-Y-Nd alloy. The microstructural evolution and superplastic behavior of the processed Mg-Y-Nd alloy were investigated at various temperature and strain rate ranges. An excellent high strain rate superplasticity was achieved at the temperature of 758K and the strain rate of 0.02/s. Maximum elongation was achieved at the temperature of 733K and the strain rate of 0.003/s. The improved superplasticity and elongation of the processed alloy are due to the grain refinement and stable microstructure imposed by the processing conditions. Mabuwa and Msomi [19] have explored the comparative performance of the friction stir welded AA8011/AA6082 dissimilar joint which was friction stir processed under two different conditions i.e., underwater and under normal air. The microstructural analysis revealed grain refinement to specimens processed underwater than those processed under normal air. The material positioning was also found to have a significant influence on the microstructural evolution of both processing conditions. Moreover, the sampling position was determined to be an important aspect for consideration when the analysis is performed on the joint. The specimens sampled at the beginning of the joint showed lower properties than the specimens sampled from other locations of the joint.

The literature shows that the FSP technique can be employed to enhance material performance, however, the recent developments show that this technique can be used to enhance the welded joints' performance [3,4,20]. However, the success of the FSP procedure depends on various parameters and almost all those parameters are directly and indirectly linked to the heat generation required for the softening and flow of material. To our best knowledge, there are very few studies that have analyzed thermal history during the submerged FSP performance, but this information is crucial as it influences various properties of the processed material. This paper reports on the relationship

between heat input (thermal history) and the microstructure of the submerged FSPed TIG-welded AA6082/AA8011 dissimilar joint. The thermal history and mechanical properties are studied in conjunction with the sampling positions.

## 2. Materials and methods

The base materials used in this study were AA6082-T6 and AA8011-H14 which were dimensioned into 260 x 52 x 6 mm. The dimensioned plates were joined together to form the dissimilar joint through the use of generic tungsten inert gas (TIG) welding. The TIG-welded joints were later subjected to the friction stir processing technique that was fully submerged underwater with a temperature that was similar to room temperature. The TIG-welding and the underwater friction stir processing procedure used in this study are similar to those reported in the literature [3,19,22]. Before the friction stir processing, the K-type thermocouples were inserted into 3 mm deep and 4 mm diameter holes that were 2 mm away from the tool path. The schematic diagram which depicts the thermocouple positioning is shown in Figure 1. The chemical composition of the two dissimilar alloys used in this study is similar to that in the literature [19,21]. The submerged friction stir processing (SFSP) parameters are a rotational speed of 1200 rpm, traverse speed of 50 mm/min, and a tool tilt angle of  $2\alpha$ . The triangular pin profile with flutes was utilized to perform SFSP on a TIG-welded AA6082/AA8011 dissimilar joint [19]. It should be noted that the SFSP was conducted with AA6082-T6 positioned on the advancing side of the tool although the thermal history was logged on both the advancing and retreating sides. The water level was maintained at 40 mm from the base of the backing plate.

The specimens were cut in different regions of the joint, i.e., start, middle, and end of the joint. The specimens were categorized according to the locations from which they were sampled: start, middle, and end of the joint. Specimens sampled within the region of thermocouples 1, 2, and 3 are called the start of the joint specimens, whereas the middle region was the region within thermocouples 4, 5, and 6. The specimens sampled at the end of the joint were the specimens sampled within the region of thermocouples 6, 7, and 8. Waterjet technology was used to prepare the specimens for mechanical analysis. The fractured surface was examined using scanning electron microscopy (SEM). The ASTM-E-384-11 standard was used to conduct microhardness tests on an InnovaTest Falcon 500 machine. The ASTM-E-8M-04 and ASTM-E-112-12 standards were used to conduct the tensile test and grain size measurement, respectively. Motic AE2000 microscopy and Hounsfield tensile testing machines were used to conduct microstructural analysis and measure tensile properties of the processed joint, respectively. The linear intercept method was used to measure the grains of the processed joint through ImageJ software. The modified Keller's reagent was used for AA8011, while Weck's reagent was used for AA6082 microstructural analysis.

## 3. Results and discussions

### 3.1 Heat input analysis

The temperature profile during SFSP was logged along the TIG-welded AA6082/AA8011 dissimilar joint. The odd-numbered thermocouples logged temperature from the retreating side (AA8011 side) of the joint while the even-numbered thermocouples logged temperature from the advancing side (AA6082 side) (Figure 2). The peak temperature at the beginning of the joint is

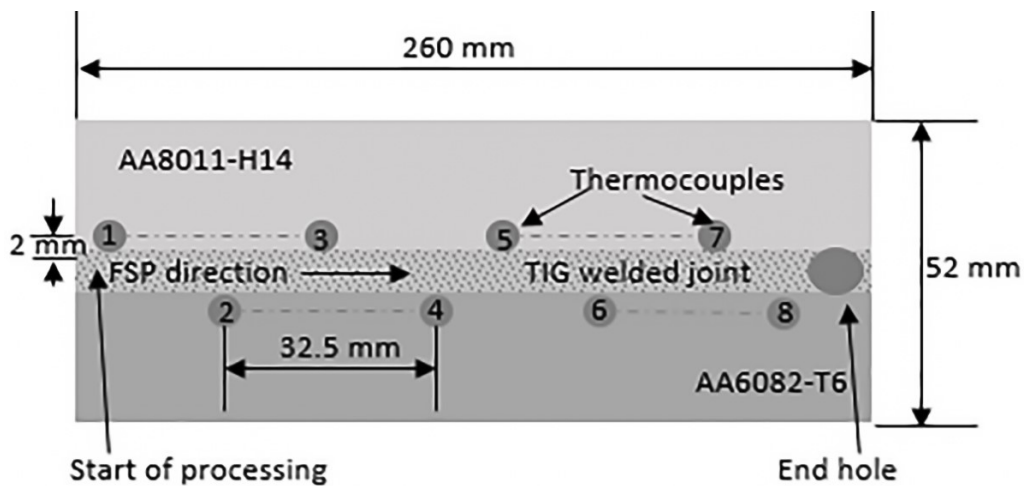


Fig. 1: Schematic diagram showing thermocouple positioning during SFSP procedure

higher than the peak temperature towards the end of the joint. However, the highest peak temperature reached during SFSP (~138 °C) is lower than the melting point of the two materials used in this study (AA8011-H14 ~ 650 °C; AA6082-T6 ~ 555 °C) [23–25]. Temperature instability is observed at the beginning of the joint (T1-T3) while uniform peak temperature is observed from the middle towards the end of the joint (T4-T8). There is no significant temperature change on the advancing and retreating sides. This suggests that the temperature distribution was uniform on both advancing and retreating sides. The peak broadness differs along the joint showing that the cooling rate decreased from the middle to the end of the joint. This is because the water circulation system was not incorporated during the SFSP procedure. There are also double peaks with different intensities observed from T1 and T2, an indication of temperature variation. This variation is suggested as emerging from the mechanical effects of the system.

### 3.2 Microstructural analysis

Figure 3 shows the microstructural grains at the stir zone (SZ) of the submerged friction stir processed TIG-welded AA8011/AA6082 dissimilar joint. Figure 3(a) shows the grain structure of the SZ for specimens sampled in the region enclosed by thermocouples T1, T2, and T3. The grain structure for the region enclosed by thermocouples T4, T5, and T6 is shown in Figure 3(b). Figure 3(c) shows the microstructure of the SZ for the region enclosed by thermocouples T6, T7, and T8. The mean grain size for the SZ for all three specimens is shown in Figure 4. The SZ shown in Figure 3(a) reveals a mixture of refined and coarsened grains while the other two stir zones (Figures 3[b] & [c]) are dominated by uniform refined grains. The mixed grain sizes observed in Figure 3(a) are attributed to the instability of heat input that was observed in Figure 2 [19,26]. The stabilization of heat input observed from the thermal history profile has resulted in the uniform distribution of grains from the middle to the end of the joint. The mean grain size at the start of the joint is higher than the mean grain size of the other two regions (Figure 4).

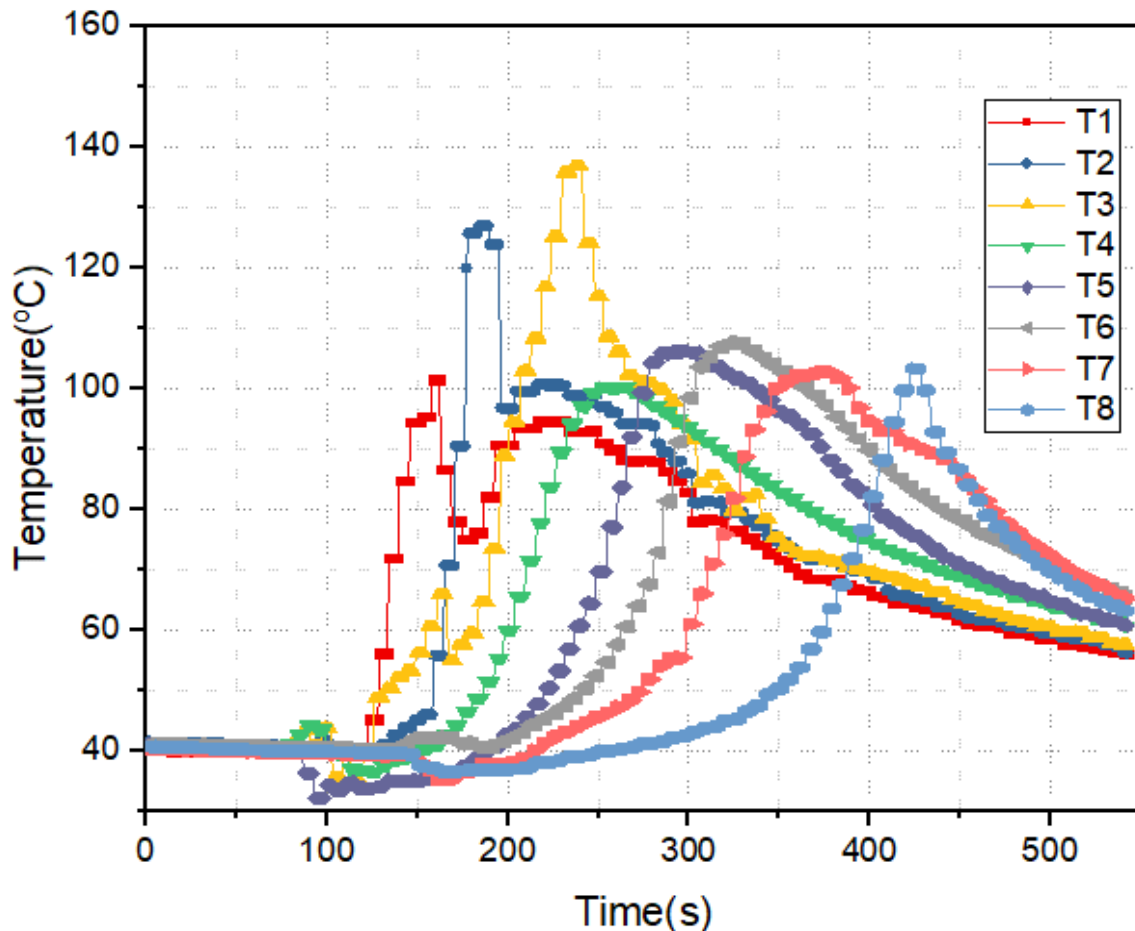
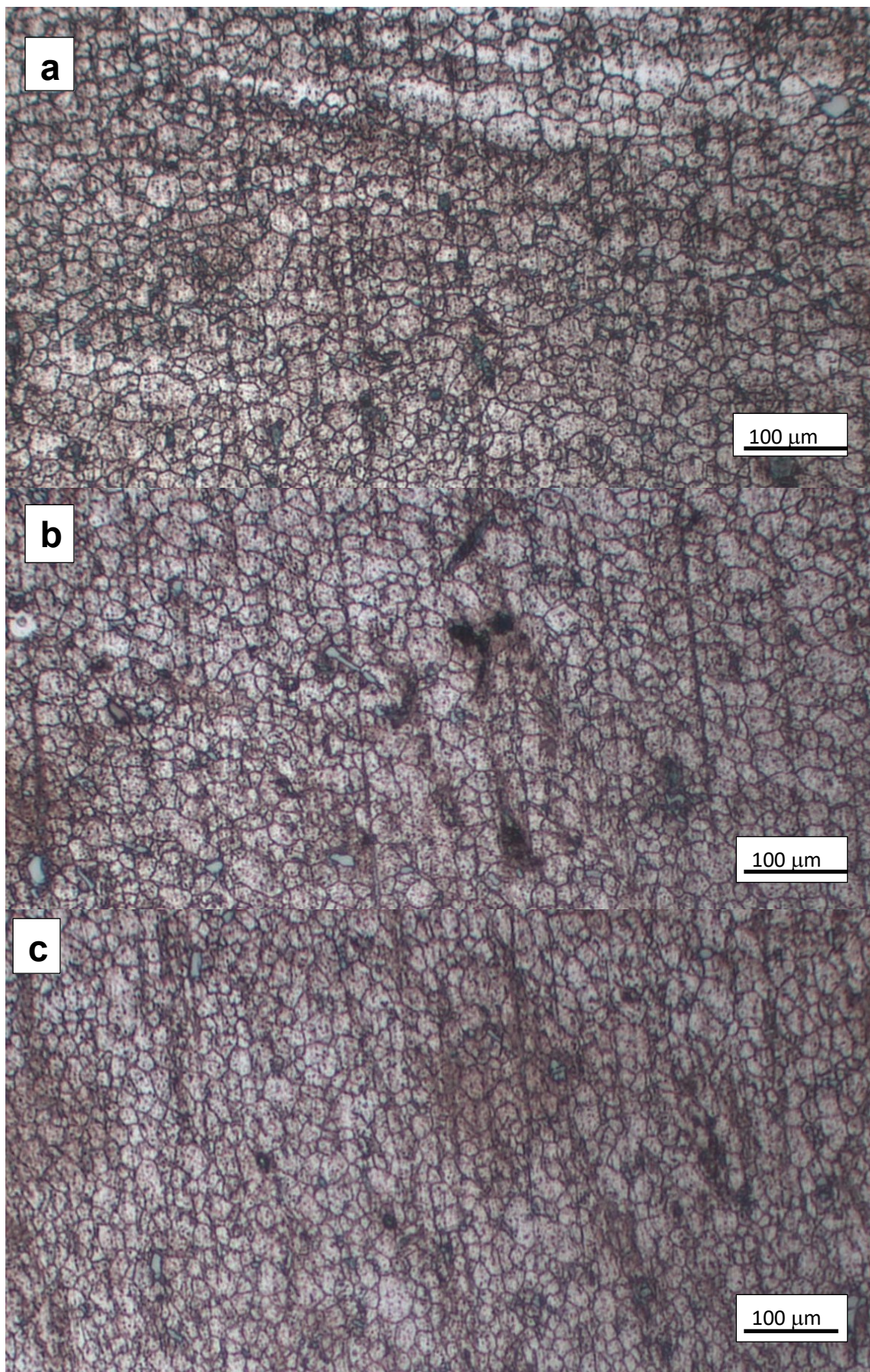


Fig. 2: Thermal profile for SFSP TIG-welded AA6082/AA8011 dissimilar joint



**Fig. 3:** Microstructural morphology at the stir zone: (a) start of joint; (b) middle of joint; (c) end of joint

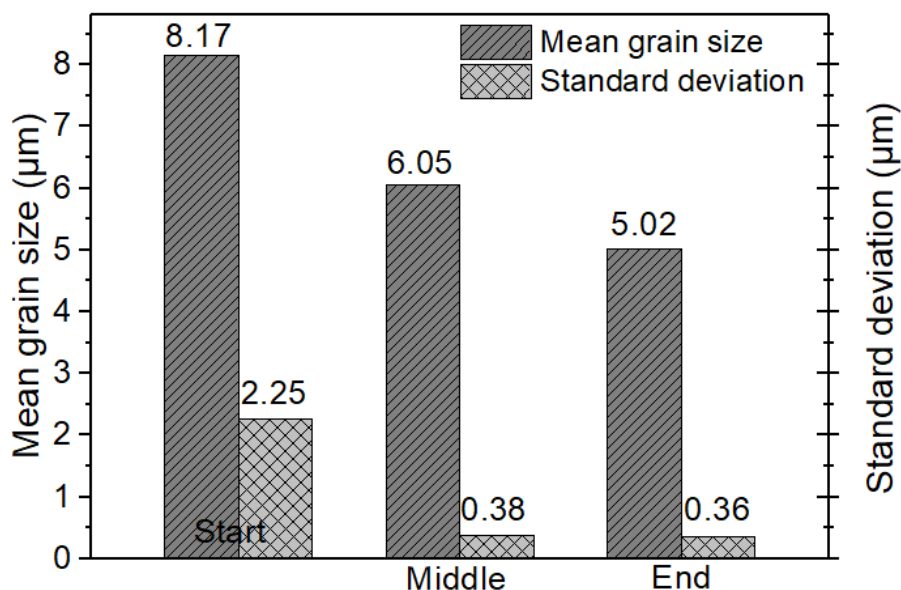


Fig. 4: Mean grain size plot

### 3.3 Tensile properties

Figure 5 shows the stress-strain curves for the specimens sampled from the start, middle, and end of SFSPed AA6082/AA8011 TIG-welded dissimilar joint. There is a linear increase in ultimate tensile strength (UTS) and the percentage elongation is observed from the start of the joint until the end of the joint. The increase in UTS and percentage elongation is attributed to the grain size refinement which depends on the stability of heat input [21,22]. The specimen sampled at the end of the joint exhibited higher tensile properties than the specimens sampled from the other locations of the SFSPed TIG-welded joint. This phenomenon is described by the Hall-Petch relationship [27]. The instability of heat input observed during thermal analysis has directly affected the tensile properties of the specimen sampled at the start of the AA6082/AA8011 TIG-welded dissimilar joint. It is observed that the UTS of all the specimens is less than both base metals. The percentage elongation of the specimen sampled from the start is less than both base materials, while the specimens sampled from the other locations have a percentage elongation higher than AA6082 but lower than AA8011. This kind of behavior, similar to that reported in the literature, is attributed to the softening mechanism [4,20,28].

### 3.4 Microhardness analysis

Figure 6 shows the microhardness profile for the specimens sampled from the start, middle, and end of the joint of the submerged friction stir processed (SFSPed) TIG-welded AA6082/AA8011 dissimilar joint. The generic zig-zag-like profile

indicating the joint that is formed using dissimilar materials is observed in Figure 6 [19,27]. The microhardness on the TMAZ region of the AA6082 side shows different paths towards the stir zone for the three specimens. The microhardness for the specimens sampled from the start and middle of the joint shows a growing trend from the thermo-mechanically heat affected zone (TMAZ) towards the stir zone, while a nonlinear profile is observed from the specimen sampled at the end of the joint. This phenomenon suggests that the TMAZ for the three specimens experienced mixed mechanisms, i.e., over-aging and coarsening of strengthening precipitates and the formation of fine precipitate distribution. Generally, the drop in microhardness for precipitate materials is attributed to the dissolution and over-aging of precipitates, whereas

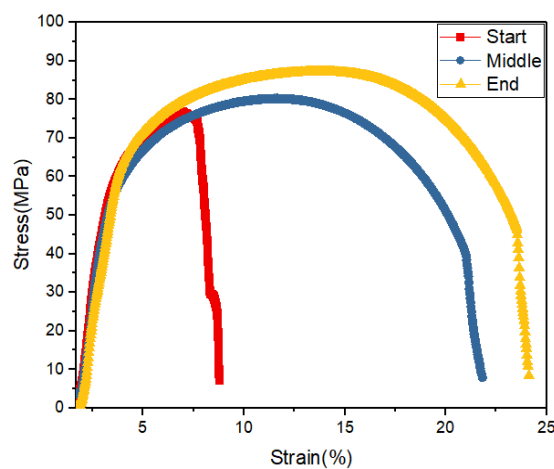


Fig. 5: Stress-strain curve for the specimens sampled from the start, middle, and end of SFSPed AA6082/AA8011 TIG-welded dissimilar joint

**Table 1:** Tensile properties of the SFSPed TIG-welded AA6082/AA8011 dissimilar joint and base materials

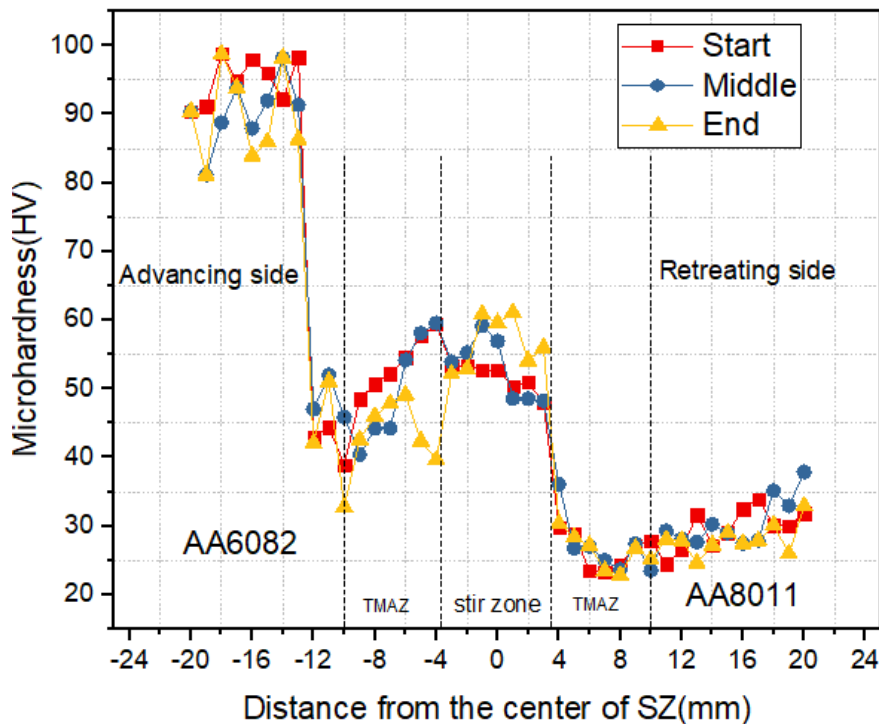
Material/Joint type	Ultimate tensile strength (MPa)	Percentage elongation
AA6082	308	19.5
AA8011	94.1	38.27
AA6082/AA8011 - S	76.9	8.79
AA6082/AA8011 - M	80.3	21.82
AA6082/AA8011 - E	87.2	24.12

the increase in microhardness suggests the formation of a fine and uniform distribution of precipitates [28,29]. The other factor that contributes towards microhardness increase is the Orowan mechanism which explains the presence of an intermetallic compound and its contribution to the microhardness increase [30]. While there is a sharp increase in microhardness for the specimen sampled at the end of the joint, a decreasing trend is observed from specimens sampled from the start and middle of the joint. However, mixed behavior is observed from the specimen sampled from the middle of the joint, and this mixed behavior is attributed to the temperature variation experienced by the location through which this specimen was sampled (Figure 2). The stir zone microhardness of the specimen sampled at the end of the joint was higher than the microhardness of the other two specimens due to the Orowan mechanism and the Hall-Petch mechanism caused by the pin stirring

action at this region [30,31]. The microhardness of all the specimens shows a decreasing trend after the stir zone. This behavior is suggested to be caused by the coarsening of grains due to the pin stirring action. The second contributing factor could be that the retreating side is dominated by AA8011 [31,32]. The microhardness of the stir zone for all the specimens is higher than that of AA8011 base material but lower than that of AA6082 base material, a behavior similar to the one reported in the literature [4,21,30,31].

### 3.5 Fractured surfaces analysis

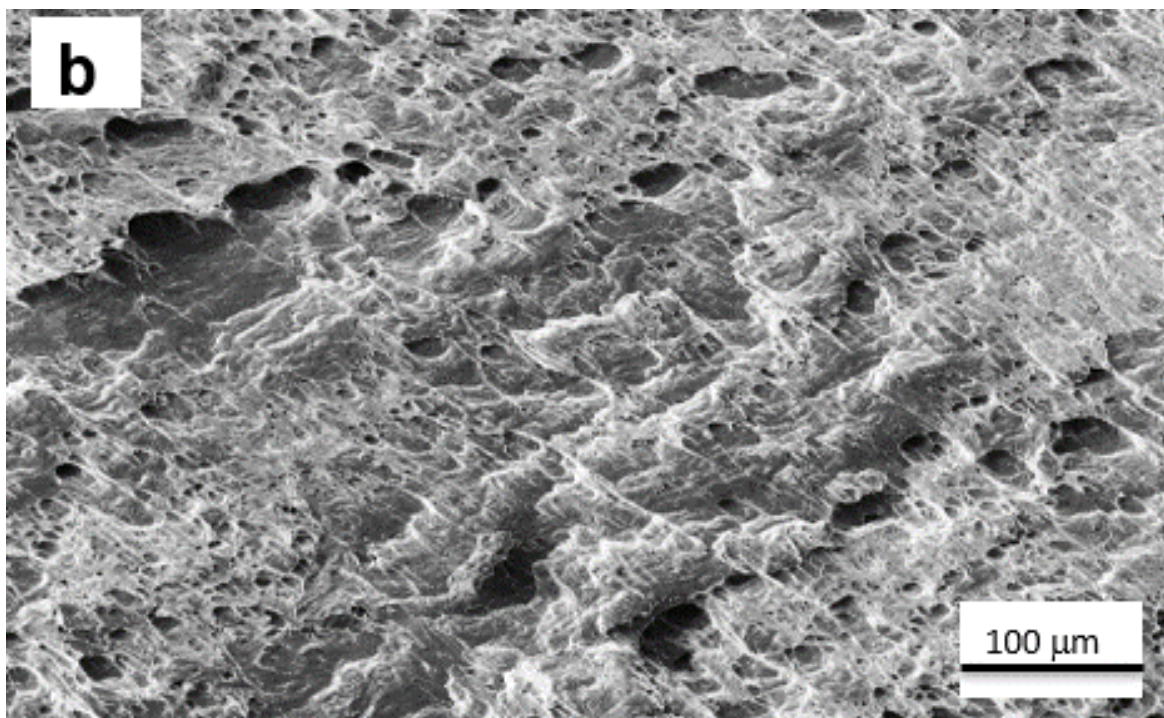
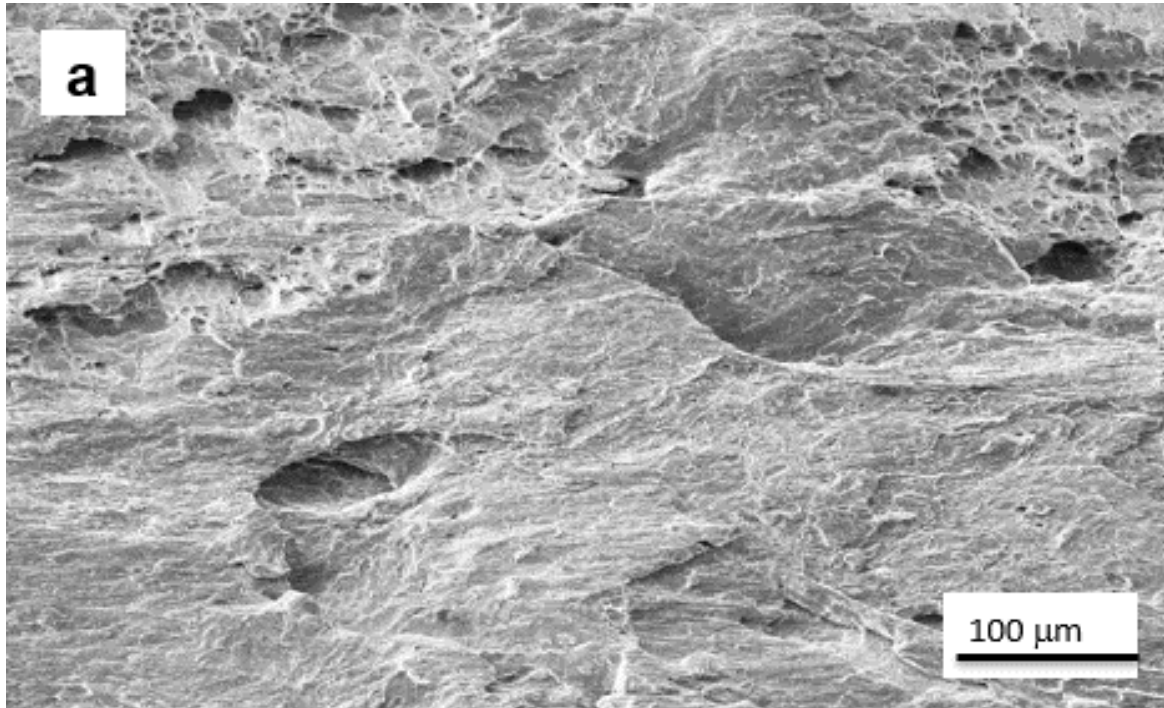
Figure 7 shows the fractured surfaces of the three specimens post-tensile testing. Figure 7(a) shows the fractured surface of the specimen sampled from the start of the AA6082/AA8011 dissimilar joint, while the fractured surfaces of



**Fig. 6:** Microhardness profile for SFSP AA8011/6082 dissimilar joint

AA6082/AA8011 dissimilar joint are shown in Figures 7(b) and 7(c). A low intensity of dimples is observed in Figure 7(a), indicating the poor bonding of material at the location of the fracture. The poor bonding is attributed to the instability of the heat input observed during thermal history analysis. The cleavage-like surfaces were also detected in Figure 7(a) and those are evidence of brittle fracture in some zones of the joint [30]. The surfaces of Figures 7(b) and 7(c) are dominated by

the presence of cup-like dimples which indicate ductile failure mode [3,4,18,30]. The dimples appearing on the surface of Figure 7(c) are finer and deeper than those in Figure 7(b). This phenomenon is due to the refinement of the grains dominating the specimen sampled from the end of the AA6082/AA8011 dissimilar joint [28,29]. The deepened dimples indicate the good quality of material bonding during processing.



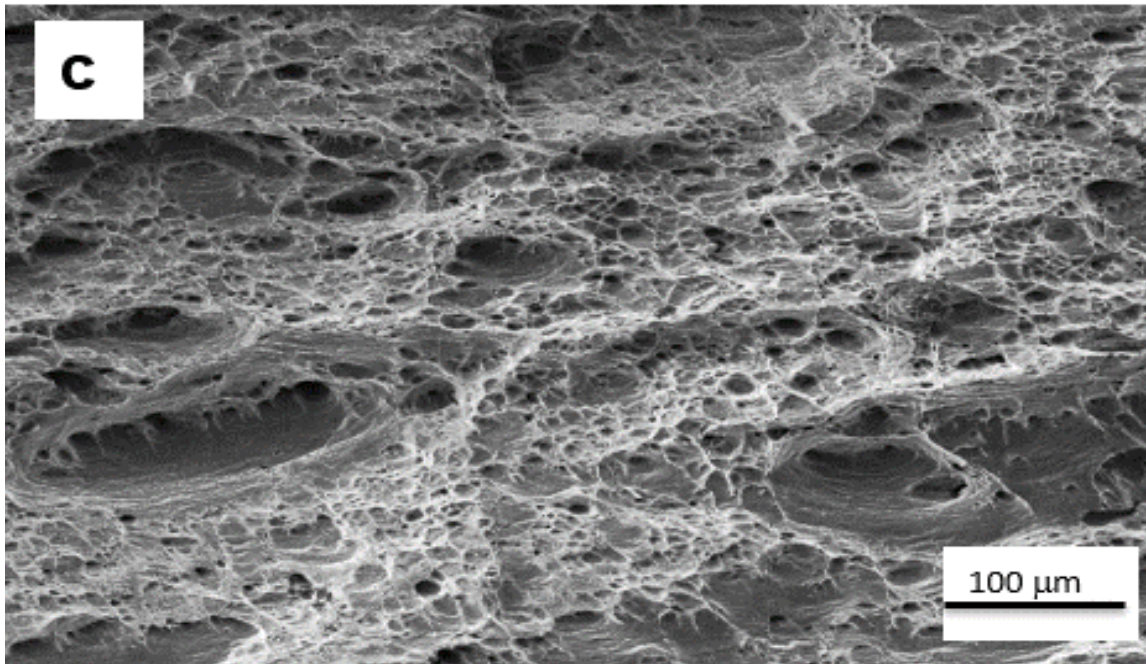


**Fig. 7:** Surface fracture morphology of specimen sampled from different locations of AA6082/AA8011 TIG-welded dissimilar joint: (a) start of joint; (b) middle of joint; (c) end of joint

#### 4. Conclusion

The correlation between the heat input and the microstructure of the submerged friction stir processed TIG-welded AA6082/AA8011 dissimilar joint was studied successfully. The following conclusions were drawn from the results:

- Thermal instability was experienced at the start of the joint, as shown by more than one peak detected by the thermocouples installed in this region (the first three sets of thermocouples). However, thermal instability subsided from the middle to the end of the joint. It was further observed that the performance of the FSP procedure underwater has assisted in keeping the maximum processing temperature below 200 °C. Keeping the processing temperature below 200 °C could have played a major role in preserving the strengthening precipitates that are influential in increasing the strength of AA6082 (precipitate material).
- The average grain size that was measured using ImageJ software showed a decrease in grain size along the joint, with larger grains size associated with the specimens sampled from the start of the joint and smaller grains measured on the specimens sampled from the middle to the end of the joint. This variation in grain size is attributed to the thermal instability that was observed during thermal history analysis.

- The tensile properties were increasing from the start to the end of the joint. The increase in tensile properties is attributed to the grain refinement that was observed during the microstructural analysis. It is good to note that the tensile properties of the joint remained relatively lower than the parent materials. The decrease in tensile properties is attributed to the dissolution of strengthening precipitates during the TIG-welding procedure.
- In summary, the variation in heat input influenced the mechanical properties of the joint.

#### 5. Conflict of interest

No conflict of interest is anticipated from this work.

#### 6. Data availability

The data used in this work is not available as this study forms part of a continuing project.

#### 7. References

- [1] Y. Chen, H. Ding, S. Malopheyev, R. Kaibyshev, Z. Cai, W. Yang, Influence of multi-pass friction stir processing on microstructure and mechanical properties of 7B04-O Al alloy, *Trans. Nonf. Met. Soc. China* 27(4)(2017): 789-796.
- [2] F. Chai, D. Zhang, Y. Li, W. Zhang, High

- strain rate superplasticity of a fine-grained AZ91 magnesium alloy prepared by submerged friction stir processing, *Mat. Sc. Eng. A* 568(2013): 40-48.
- [3] S. Mabuwa, V. Msomi, Effect of Friction Stir Processing on Gas Tungsten Arc-Welded and Friction Stir-Welded 5083-H111 Aluminium Alloy Joints. *Adv Mater Sci Eng.* (2019): 3510236.
- [4] S. Mabuwa, V. Msomi, The effect of friction stir processing on the friction stir welded AA1050-H14 and AA6082-T6 joints, *Mat. Today: Proc* 26(2)(2020): 193-199.
- [5] A. Kurt, I. Uygur, E. Cete, Surface modification of aluminium by friction stir processing, *J. Mat. Proc. Tech* 211(3)(2011): 313-317.
- [6] M. Sudhakar, C.S. Rao, K.M. Saheb, Production of Surface Composites by Friction Stir Processing-A Review, *Mat. Today: Proc.* 5(1)(1)(2018): 929-935.
- [7] G. Huang, J. Wu, W. Hou, Y. Shen, Microstructure, mechanical properties and strengthening mechanism of titanium particle reinforced aluminum matrix composites produced by submerged friction stir processing, *Mat. Sc. Eng A* 734(2018): 353-363.
- [8] H.Seifiyan, M.H. Sohi, M. Ansari, D. Ahmadkhaniha, M. Saremi, Influence of friction stir processing conditions on corrosion behavior of AZ31B magnesium alloy. *J Magnes Alloy* 7(4)(2019): 605-616.
- [9] S. Bharti, V. Dutta, S. Sharma, N.D. Ghetiya, Investigating the effect of tool speed on the mechanical properties of Al5052 processed by friction stir processing. *Mater Today Proc* (2020); In Press.
- [10] C. Chanakyan, S. Sivasankar, M. Meignanamoorthy, M. Ravichandran, T. Muralidharan, Experimental investigation on influence of process parameter on friction stir processing of AA6082 using response surface methodology. *Mater Today Proc* 21(21)(1)(2020): 231-236.
- [11] C.Y. Ma, L. Zhou, R.X. Zhang, D.G. Li, F.Y. Shu, X.G. Song, Y.Q. Zhao, Enhancement in mechanical properties and corrosion resistance of 2507 duplex stainless steel via friction stir processing. *J Mater Res Technol* 9(4)(2020): 296-305.
- [12] X. Yang, Z. Yan, P. Dong, B. Cheng, J. Zhang, T. Zhang, H. Zhang, W. Wang. Surface modification of aluminum alloy by incorporation of AlCoCrFeNi high entropy alloy particles via underwater friction stir processing. *Surf Coatings Technol.* 385(2020): 125438.
- [13] P. Xue, B.L. Xiao, Z.Y. Ma. Achieving Large-area Bulk Ultrafine Grained Cu via Submerged Multiple-pass Friction Stir Processing. *J Mater Sci Technol.* 29(12)(2013): 1111-1115.
- [14] X. Feng, H. Liu, J.C. Lippold, Microstructure characterization of the stir zone of submerged friction stir processed aluminum alloy 2219. *Mater Charact* 82(2013): 97-102.
- [15] F. Chai, D. Zhang, Y. Li Y, Microstructures and tensile properties of submerged friction stir processed AZ91 magnesium alloy. *J Magnes Alloy* 3(3)(2015): 203-9.
- [16] K. Selvam, A. Prakash, H.S. Grewal, H.S. Arora. Structural refinement in austenitic stainless steel by submerged friction stir processing. *Mater Chem Phys* 197(2017): 200-207.
- [17] B. Darras, E. Kishta, Submerged friction stir processing of AZ31 Magnesium alloy. *Mater Des.* 47(2013): 133-137.
- [18] G. Cao, D. Zhang, F. Chai, W. Zhang, C. Qiu, Superplastic behavior and microstructure evolution of a fine-grained Mg-Y-Nd alloy processed by submerged friction stir processing. *Mater Sci Eng A* 642(2015): 157-166.
- [19] S. Mabuwa, V. Msomi, Comparative analysis between normal and submerged friction stir processed friction stir welded dissimilar aluminium alloy joints. *J Mater Res Technol* 9(5)(2020): 9632-9644.
- [20] H. Mehdi, R.S. Mishra. Effect of Friction Stir Processing on Microstructure and Mechanical Properties of TIG Welded Joint of AA6061 and AA7075. *Metallogr Microstruct Anal* 9(3)(2020): 403-418.
- [21] S. Mabuwa, V. Msomi. 2020. Fatigue behaviour of the multi-pass friction stir processed AA8011-H14 and AA6082-T651 dissimilar joints. *Eng Fail Anal* 118, 104876.
- [22] S. Mabuwa, V. Msomi. 2020. The impact of submerged friction stir processing on the friction stir welded dissimilar joints, *Mat Res Express* 7(9), 096513.

- [23] K. Navneet, B. Mahesh, P. Sharma, V.J. Badheka, Design-of-experiments application in the friction stir welding of aluminium alloy AA 8011-h14 for structural application. *Multidiscip Mode I Mater Struct* 16(3)(2019): 606-622.
- [24] N. Khanna, P. Sharma, M. Bharati, V.J. Badheka. Friction stir welding of dissimilar aluminium alloys AA 6061-T6 and AA 8011-h14: a novel study. *J Brazilian Soc Mech Sci Eng* 42(2019): 7.
- [25] D. Birsan, E. Scutelnicu, D. Visan. Behaviour Simulation of Aluminium Alloy 6082-T6 during Friction Stir Welding and Tungsten Inert Gas Welding. *Int Conf Manuf Eng Qual Prod Syst MEQAPS - Proc. 2011 Jan 1*.
- [26] V. Msomi, N. Mbana. Mechanical properties of friction stir welded AA1050-H14 and AA5083-H111 joint: Sampling aspect. *Metals* 10(2)(2020): 214.
- [27] M. Paidar, V.R. Vaira, A. Khorram, O.O. Ojo, A. Rasoulpouraghdam, I. Pustokhina. Dissimilar modified friction stir clinching of AA2024-AA6061 aluminum alloys: Effects of materials positioning. *J Mater Res Technol.* 9(3)(2020): 6037-6047.
- [28] M.D. Sameer, A.K. Birru. Mechanical and metallurgical properties of friction stir welded dissimilar joints of AZ91 magnesium alloy and AA 6082-T6 aluminium alloy. *J Magnes Alloy.* 7(2)(2019): 264-271.
- [29] S.T. Azeez, E.T. Akinlabi. Effect of processing parameters on microhardness and microstructure of a double-sided dissimilar friction stir welded aa6082-t6 and aa7075-t6 aluminum alloy. *Mater Today: Proc* 5(9)(3)(2018): 18315-18324.
- [30] B. Safarbali, M. Shamanian, A. Eslami, Effect of post-weld heat treatment on joint properties of dissimilar friction stir welded 2024-T4 and 7075-T6 aluminum alloys. *Trans Nonferrous Met Soc China* 28(7)(2018):1287-1297.
- [31] C. Sharma, D.K. Dwivedi, P. Kumar, Influence of pre-weld temper conditions of base metal on microstructure and mechanical properties of friction stir weld joints of Al-Zn-Mg alloy AA7039. *Mater Sci Eng A* 620(2015): 107-119.
- [32] P. Cavaliere, A. De Santis, F. Panella, A. Squillace, Effect of welding parameters on mechanical and microstructural properties of dissimilar AA6082-AA2024 joints produced by friction stir welding. *Mater Des* 30(3)(2009): 609-16.
- [33] M. Cabibbo, H.J. McQueen, E. Evangelista, S. Spigarelli, M. Di Paola, A. Falchero, Microstructure and mechanical property studies of AA6056 friction stir welded plate. *Mater Sci Eng A.* 460-461(2007): 86-94.